Zhang *et al. Heritage Science* (2022) 10:202
https://doi.org/10.1186/s40494-022-00845-9

Heritage Science

RESEARCH

Open Access

Characterization of degradation and iron deposits of the wood of Nanhai I shipwreck

Hongying Zhang[1], Dawa Shen[2], Zhiguo Zhang[3] and Qinglin Ma[4*]

Abstract

Nanhai I shipwreck was a large wooden merchant ship (22.15 m in length and 9.85 m in width) built in the Southern Song Dynasty (1127–1279 A.D.) of China, which was heavily loaded with a large number of porcelain and iron artifacts. In the South China Sea, it was found in 1987 and lifted as a whole in 2007. Its excavation provides a precious opportunity to reveal the preservation status of Nanhai I shipwreck. Iron compounds give rise to challenges in conservation procedures and the long-term stability of Nanhai I shipwreck. In this paper, the degradation of the wood and the iron deposits in the wood structure are investigated from the aspects of microscopic morphology, composition, and distribution to evaluate the preservation state of the waterlogged wood. Physical parameters, chemical composition, and the results of elemental analysis, and FTIR analysis suggest that the cellulose of wood is degraded, and the relative concentration of lignin increases. The ash content varies greatly among different samples, and the element of the highest content in ash is iron. The study on transverse and longitudinal sections from samples indicate that the deposits are unevenly concentrated in the cell lumen, middle lamella, rays, and pits of the cell wall. The cell lumen is filled with deposits in areas close to the surface of the samples. The XRD analysis demonstrates that the deposits in wood are mainly iron deposits, containing compounds pyrite (FeS_2), siderite ($FeCO_3$), iron oxyhydroxides (FeOOH), and magnetite (Fe_3O_4). The micro-X-ray Fluorescence mapping analysis suggests that the content of iron is relatively richer while containing less sulfur on the exterior of the sample. The presence of iron deposits accelerates wood degradation and increases the safety hazards of shipwrecks in the preservation process. We hope that our findings can make a modest contribution to iron removal from waterlogged archeological wood and shipwreck conservation.

Keywords: Nanhai I shipwreck, Marine archaeological wood, Waterlogged wood, Degradation, Iron deposits

Introduction

Nanhai I, an ancient Chinese merchant ship of the Southern Song Dynasty (1127–1279 AD), sank about 19 km southwest to Xiachuan Island and about 23 km off the coast of Guangdong Province. The shipwreck was discovered in the 1980s, then salvaged integrally in 2007. Now Nanhai I shipwreck is being preserved in Guangdong Maritime Silk Road Museum. Excavation of Nanhai I began in 2013 and is still ongoing. The protection of Nanhai I shipwreck is still ongoing. A total of 180,000 pieces of artifacts including porcelain, metalware, gold jewelry, silver, copper, lead, tin, lacquerware, glassware, etc. have been extracted [1]. Iron artifacts from Nanhai I shipwreck mainly included trade products, such as iron pots and iron nail raw materials. Iron pots and iron nail raw materials were regularly placed in 9 cabins of Nanhai I shipwreck (Fig. 1). Due to the erosion in seawater for more than 800 years, a large number of densely placed iron artifacts have been corroded, and formed concretions by the iron corrosion products interacting with material adjacent to the iron [1, 2]. More than 130 tons of iron artifacts and concretions have been extracted. Iron compounds formed on the surface of the cabin and inside the wood structure. The hull is unevenly polluted by iron

*Correspondence: qinglinma226@126.com

[4] International Joint Research Laboratory of Environmental and Social Archaeology, Shandong University, Qingdao 266237, Shandong Province, China
Full list of author information is available at the end of the article

Fig. 1 Orthophoto of Nanhai I shipwreck (Red area is the location of iron pots and nail raw materials in the cabin)

corrosion, and partially mineralized, which seriously affects the later protection of the shipwreck.

Iron deposits are widely found in marine archaeological wood (Table 1). The analysis of deposits in the wood of the Swedish Vasa shipwreck showed that iron (1–10 mg/g) below the surface of the wood was mainly in the form of Fe (II) and Fe (III) compounds [3]. Study on sulfur and iron morphology in a wood sample of Mary Rose in the United Kingdom demonstrated that iron and sulfur could be found co-existing only in iron sulfide grains. Iron corrosion products mainly existed in the cell walls, whereas organic sulfur compounds in the middle lamella [4, 5]. The analysis of the wood of the Italian Roman ships Pisa L reported that the mineral elements in the wood were sulfur, calcium, and iron. Iron existed in the form of $FeSO_4{\cdot}H_2O$, which might be related to the oxidation of iron nails in the ship structure [6]. Compounds such as FeOOH, FeS_2, $FeSO_4$, and $FeCO_3$ were detected on the surface of the wreck of La Natière and Gallo-Roman in France [7].

In China, plenty of deposits were found in marine archaeological shipwrecks. Deposits in most of the wood structure of Quanzhou Ship of the Song Dynasty were iron compounds. Most of the iron compounds were in the oxidized state, such as $KFe_3(SO_4)_2(OH)_6$, $NaFe_3(SO_4)_2(OH)_6$, and $Fe_2(CO_3)_3$. Our team analyzed the characteristics of deposits in the wood structure of Nanhai I shipwreck in 2011 and 2014. The analysis of the wood of Nanhai I shipwreck showed that the iron deposits are composed of FeOOH, $KFe_3(SO_4)_2(OH)_6$, and FeS_2 [10]. The analysis of the wood of Huaguangjiao I and its surface attachments showed that the iron deposits are composed of FeOOH, $KFe_3(SO_4)_2(OH)_6$, and a small number amount of Fe_2O_3, FeS_2, $FeSO_4{\cdot}4H_2O$, $FeSO_4{\cdot}7H_2O$ [11]. FeS_2 was found both in the deposits of the shipwreck of Nan'ao I and Xiaobaijiao I shipwreck [12, 13].

During the burial of the shipwreck, iron from seawater and artifacts as well as sulfates in seawater had generated a large number of iron sulfide compounds, such as FeS, FeS_2, and Fe_3S_4, under the action of microorganisms, and

Table 1 Type of deposits in the waterlogged archaeological woods

Shipwrecks	Salvaged time	Deposits		Diagnostic techniques	References
		Iron deposits	Others		
Vasa	1961	$FeSO_4{\cdot}7H_2O$, $KFe_3(SO_4)_2(OH)_6$, $NaFe_3(SO_4)_2(OH)_6$	$CaSO_4$	SEM–EDS, XAFS	[3]
Mary Rose	1982	FeS_2, Fe_8S_9, Fe_2O_3, $FeSO_4{\cdot}4H_2O$, $FeSO_4{\cdot}7H_2O$, $NaFe_3(SO_4)_2(OH)_6$, $KFe_3(SO_4)_2(OH)_6$	$CaSO_4{\cdot}2H_2O$ $CaCO_3$	SEM, XANES, XRD, EXAFS	[4, 5]
Pisa-L	2003	$FeSO_4{\cdot}H_2O$	$CaSO_4{\cdot}2H_2O$ $CaSO_4{\cdot}0.5H_2O$	XRD, SEM–EDX	[6]
La Natière Gallo-roman	2006	FeS_2, FeOOH, $FeSO_4{\cdot}4H_2O$, $FeCO_3$, $NaFe_3(SO_4)_2(OH)_6$	–	ESEM-EDS, μ-RS	[7]
Batavia	1971	FeS, FeS_2, FeOOH, $Fe(OH)_2$, $FeSO_4{\cdot}4H_2O$, $FeSO_4{\cdot}5H_2O$, $KFe_3(SO_4)_2(OH)_6$, $NaFe_3(SO_4)_2(OH)_6$	–	XRD	[8]
Lyon Saint-Georges 4	2003	FeS_2, Fe_3S_4	–	ESEM-EDX, μ-RS, XRD	[9]
Quanzhou Ship	1974	FeS_2, $Fe_2(CO_3)_3$, $KFe_3(SO_4)_2(OH)_6$, $NaFe_3(SO_4)_2(OH)_6$	$CaCO_3$	XRD, SEM–EDS	[10]
Nanhai I	2007	FeS_2, FeOOH, $KFe_3(SO_4)_2(OH)_6$	–	XRD, SEM–EDS	
Huaguangjiao I	2008	Fe_2O_3, FeS_2, Fe_3S_4, FeOOH, $FeSO_4{\cdot}4H_2O$, $FeSO_4{\cdot}7H_2O$, $KFe_3(SO_4)_2(OH)_6$,	$CaSO_4{\cdot}2H_2O$, $CaCO_3$, $(Ca,Mg)(CO_3)_2CaHPO_4{\cdot}2H_2O$,$CaF_2$,$MnCO_3$,S	XRD, SEM–EDS, XPS	[11]
Xiaobaijiao I	2014	FeS, FeS_2	–	SEM–EDS, XRD	[12, 13]
Nan'ao I	2010	FeS_2	$Ca_3Al_2O_6$	SEM–EDS	

had easily deposited into marine archaeological wood. After recovery and excavation, the iron sulfide compounds exposed to the oxygen are gradually oxidized into iron (hydrogen) oxide compounds such as FeOOH, Fe_2O_3, and Fe_3O_4 and form sulfuric acid, resulting in the degradation of cellulose [14, 15]. When the increase or decrease of humidity of the preservation and exhibition of the environment, the dissolution/crystallization of different deposits occurs and causes stress cracks in wood structure [16].

PEG has become an important material for the stability of the dimensions of waterlogged wood. However, degradation of PEG has been observed in the wood of the Swedish warship Vasa and is highly correlated to the presence of iron compounds [17].

Although deionized water spraying measures have been taken to delay the acidification after the excavation and salvaging of Nanhai I shipwreck, the stability and protection work of the shipwreck have been seriously affected due to the presence of iron deposits.

Nanhai I is a salvaged shipwreck as a whole, and accordingly, its future conservation work is mainly focused on the overall protection of the shipwreck. The presence of iron deposits in shipwreck wood has seriously affected the later protection work. The analysis of loose wood, in this work, can provide a reference for the degradation degree and the characteristics of deposits in the structure of hull wood and waterlogged wood artifacts. The goal of this study is, using multiple means, characterization of degradation and deposits of the wood of Nanhai I shipwreck, to understand comprehensively. In this study, the wood degradation of Nanhai I shipwreck was evaluated by physical parameters, chemical analysis, and Fourier transforms infrared spectroscopy (FTIR). Inductively coupled plasma mass spectrometry (ICP-MS) was applied to analyze inorganic elements in wood ash. In addition, the morphology of deposits in wood structures was observed through optical microscopy. SEM–EDS and XRD were introduced to analyze the composition of deposits. Micro-X-ray fluorescence (XRF) mapping was used to analyze iron and sulfur distribution and relative content in wood. The study would provide helpful information to select the appropriate preservation method, such as removing the iron deposits, consolidantion, and dehydration of Nanhai I shipwreck.

Materials and methods

Materials

All samples are from the loose wood of Nanhai I shipwreck. The function of the loose wood was to fix between shipments of porcelains or iron artifacts to prevent collision during shipment transportation of Nanhai I shipwreck. A large number of loose wood samples were unearthed during the excavation of Nanhai I shipwreck. The loose wood was contaminated by iron deposits in different degrees. After excavation, according to the contamination degree of iron corrosion products, the loose wood was immersed in deionized water to remove soluble salt, or in EDTA-2Na solution to remove insoluble iron compounds. The samples were chosen from different contamination degrees of loose wood as the research object. Samples K2NH-1 and K2NH-2 were taken from the silt layer at the bottom of the shipwreck and analyzed after being cleaned by ultrapure water rinsing to remove the surface silt. Samples K2NH-8, K2NH-10, and K2NH-13 were soaked in deionized water before sampling. Before analysis, sample K2NH-11 was soaked in 10 mmol/L EDTA-2Na solution for 20 months. EDTA-2Na solution was replaced every 6 months. Based on the degree of deposits attached, samples can be divided into three categories: without obvious deposits attachment on the surface (sample K2NH-13), with significant deposits attachment (samples K2NH-2, K2NH-8, and K2NH-11), and mineralized seriously (sample K2NH-1 and K2NH-10) (Fig. 2).

Methods

In order to explain the degradation degree of wood and characteristic of deposits in wood structures from different perspectives, several analytical methods were applied in this study.

According to Chinese national standards of wood [18], the physical properties (saturated water quality, saturated water volume, maximum water content (MWC), and basic density (BD)) were determined. Residual basic density (RBD) was calculated as a percentage of BD between the samples and sound wood [19].

The excavation of the Nanhai I shipwreck has been lasted for 9 years and is still ongoing. Since the excavation of Nanhai I shipwreck, 5% PEG400 solution has been sprayed as a temporary method to keep wood wet and

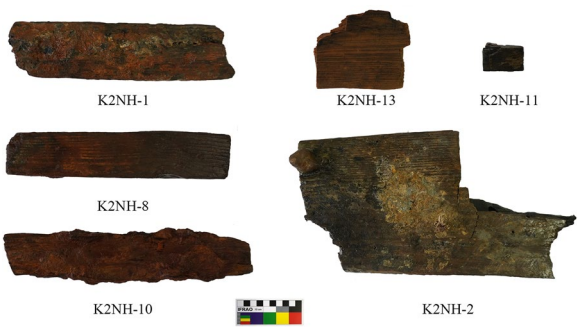

Fig. 2 Wood samples of Nanhai I shipwreck

prevent wood shrinkage, resulting in a large amount of PEG residue inside the wood structure. Since the existence of PEG may lead to some errors in the measurement results, pre-treating procedures were taken to remove it: an appropriate amount of wood was taken from the sample, ground into powder, and removal of PEG in powder by filtration multiple times using deionized water. The powder is freeze-dried under a vacuum and used for chemical components and element analysis of wood. Chinese national standards [20] of the method of fibrous raw material are recognized as also being applicable and were individually analyzed of chemical components of wood (ash, α-cellulose, acid-insoluble lignin, phenyl alcohol extract, hot water extract, etc.) of waterlogged wood. GB/T 2677 3-93 referred to the standard TAPPI T211 om-85 and was used to determine the ash content. GB/T 744-1989 referred to the standard ISO 699:1982 and was used to measure cellulose content. GB/T 2677.10-1995 was used to measure holocellulose content. GB/T 2677 4-93 referred to the standard TAPPI T207 om-88 was used to determine the content of hot water extract. GB/T 2677 8-94 referred to the standard TAPPI T222 om-88 was used to determine the acid insoluble lignin. GB/T 2677 6-99 referred to the standard TAPPI T204 om-88 was used to determine phenyl alcohol. The ratios of holocellulose and lignin (H/L) are also presented, which are good indicators reflecting the degree of wood degradation and avoiding the effects of the ash content [21]. The holocellulose content of samples was calculated according to the method of holocellulose in wood raw materials containing ash in GB/T 2677.10-1995 [20].

The composition of inorganic elements (iron, calcium, aluminum, magnesium, potassium, manganese) and sulfur in the ash were determined by inductively coupled plasma mass spectrometry (ICP-MS, PlasmaQuant MS, Analytikjena). The ashed sample is in a powder state. The sample processing for ICP-MS analysis is as follows: (1) 40 mg sample is accurately weighed and placed in Teflon sample dissolving bomb; (2) 0.5 ml high-purity HNO_3 and 1 ml high-purity HF are added successively and slowly; (3) Put Teflon sample dissolving bullet into digestion bomb, put it in the 190 ℃ oven after tightening for more than 48 h; (4) Cool the sample dissolving bullet, and then add 5 ml 30% HNO_3, put Teflon sample dissolving bullet into steel sleeve again, tighten it and put it in 150 ℃ oven overnight; (5) Transfer the solution into polyethylene plastic bottle, add Rh internal standard, and dilute it to 100 g with 2% HNO_3 for ICP-MS test. Rh internal standard was added to effectively correct instrument drift. The weight of solution was used to ensure the dilution multiple and avoid the error of volume calculation.

The elements C, H, N, S, and O of wood samples were analyzed by means of the Vario MACRO cube elemental analyzer from Elementar. Reaction conditions: the Analyzer's O_2 gas output pressure was set at 0.20–0.22 Mpa; He gas output pressure at 0.12–0.13 Mpa; combustion tube temperature at 1150 °C, reduction tube temperature at 850 °C.

Fourier transform infrared(FTIR) spectroscopy was collected on a Nicolet 670 infrared spectrometer. 2 mg of wood sample was taken, mixed with potassium bromide in the ratio of 1:100, and pressed into tablets.

Leica DM4000M optical microscope was adopted to observe the distribution and microscopic morphology of deposits of cross section and tangential section of wood sample. The slides of wood samples were handmade by cryosection and observed by a transmission light microscope. The slicing method was as follows: The samples of water saturated wood were placed on the freezing table at −20 °C temperature. In order to embed the sample into the ice, small amount of ultrapure water was added to the surface of the sample. The sample block was sliced after it was completely frozen. Slices were made and immediately placed in a glass slide containing ultrapure water drops. Coverslip was added to avoid dehydration of slices. The slices were observed under a transmission light microscope.

Rigaku's smart lab X-ray diffraction (XRD) analyzer was applied to analyze the phases of inorganic compounds of deposits in the wood; kβ filter ID for Cu; the range is 5°–80°; the step is 0.01. The morphology and composition of deposits in wood were analyzed by a Czech Tescan Vega3 SEM and a Bruker XFLASH 5000 spectrometer.

The Bruker M6 JETSTREAM micro-X-ray Fluorescence (micro-XRF) was used to analyze the distribution and relative content of the deposits in the transverse surface of the sample and the cross-section 2 cm from the surface. The excitation source was Rh target, the test condition voltage 40 kV, the current 380 μA, the spot size 100 μm, the step length is 80 μm, and the single point acquisition time 150 ms.

Results and discussion

Degradation of waterlogged archaeological wood

The six samples used for analysis are all pine (Pinaceae Pinus sp.). The main features are distinct growth rings, gradual transition from earlywood to latewood, and bordered pits in radial and tangential walls of tracheids being usually uniseriate. Uniseriate and fusiform rays are present with ray tracheids. Axial, radial resin canals and cross-field pits window-like are present (Fig. 3).

The determination of physical and chemical properties of the archeological wood can be used to assess wood degradation degree in buried environment [21, 22]. The analysis results of the physical properties (MWC, BD, and RBD) of the samples are shown in Table 2. The

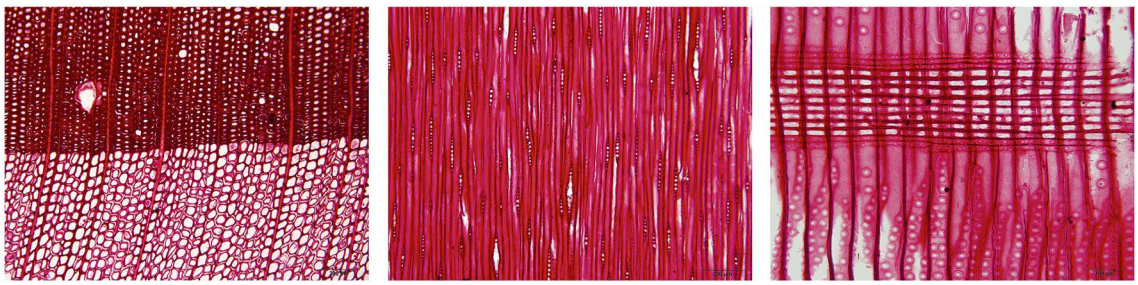

Fig. 3 Sample slice micrograph of K2NH-2

Table 2 Results of physical and chemical characterization

Sample	Maximum water content (100%)	Basic density (g/cm^3)	Residual basic density (%)	pH	H/L
K2NH-1	582.1	0.1525	38.1	7.2	0.4
K2NH-2	434.2	0.1978	49.5	7.4	0.6
K2NH-8	641.1	0.1303	32.6	3.8	0.5
K2NH-10	104.2	0.6307	157.7	3.9	1.3
K2NH-11	298.1	0.2893	72.3	4.4	0.6
K2NH-13	523.6	0.1718	42.9	6.2	0.6
Sound pine wood	–	0.4445	–	4.3	3.0

MWC is about between 104.2 and 641.1%, and the BD is about between 0.1303 and 0.6307 g/cm^3. The MWC of four samples is higher than 400%, MWC of one sample is close to 300%. Sample K2NH-10 showed a very low MWC (104.2%), high BD (0.6307 g/cm^3), and high RBD (157.7%). Based on MWC values of pine according to McConnachie Glenn et al. [23], the wood degradation of Nanhai I is degraded (MMC > 250%), except for K2NH-10. As the waterlogged wood decay develops, the mass of wood substance forming the cell wall decreases. This process results in a decrease in BD and an increase in MWC [24]. The density of iron deposits in wood is higher than the wood substance density [25]. Therefore, the result of BD and MWC of sample K2NH-10 is related to the effects of iron deposits. With visual inspection, it could be seen sample K2NH-10 was mineralized seriously. The MWC and RBD results indicate that the wood of Nanhai I shipwreck degraded greatly.

Compared to sound pine wood, the content of hot water extractive (1.2–5.3%) and benzene-alcohol extractive (1.5–7.4%) of the wood samples is relatively low, indicating that most of the low-molecular-weight extractives are lost. Considering the content of ash in waterlogged archaeological wood affects the content of α-cellulose, holocellulose, and insoluble lignin [26], the content of α-cellulose, holocellulose, and insoluble lignin in the samples were corrected according to Chinese national standards [20, 21, 23]. The results are shown in Fig. 4. The α-cellulose content (14.6–4.3%) is lower than that of sound pine wood (42.3%) [27, 28]. The insoluble lignin content (76.1–32.1%) is higher than that of sound pine wood (21.3%) [28]. A decrease in the H/L ratios confirmed a loss of carbohydrates [21] in all samples.

Moreover, the ash content of samples (1.6–37.9%) is abnormally high and varies greatly between different samples. The sample K2NH-11 from EDTA-2Na solution immersion tank exhibit a very high ash content (37.9%) and is higher than that of other samples. The sample K2NH-13 from deionized water is a lower ash content (1.6%) than that of other samples. This is relevant to whether the burial environment is close to iron artifacts and concretions. According to the ICP-MS results, the element with the highest content in ash is iron, the second one is sulfur (Table 3). The results of ash content and ICP-MS indicate iron deposits had been diffused in the wood structure during the burial of Nanhai I shipwreck.

The results of the analysis of elements C, H, O, N, and S are shown in Table 4. According to the literature, the percentages of elements C, H, O, N, and S in dry sound pine wood are respectively 49.9%, 6.3%, 42.9%, 1.0% [27], and 0.2% [28]. Compared with sound wood, the content of H and N in all samples is lower. The content of S in all samples was between 3.1 and 8.0%, which is higher than that of sound pine wood. Except for samples K2NH-2 and K2NH-13, the content of C is lower. The decrease in the ratio of oxygen to carbon (O/C) and content of H is characteristic of the degradation of carbohydrates and preservation of lignin [26, 29, 30]. The analysis results showed that the ratio of O/C gradually decreased with the increased content of holocellulose.

The pH values of samples K2NH-8 and K2NH-10 are lower than sound pine wood, and the pH values of other

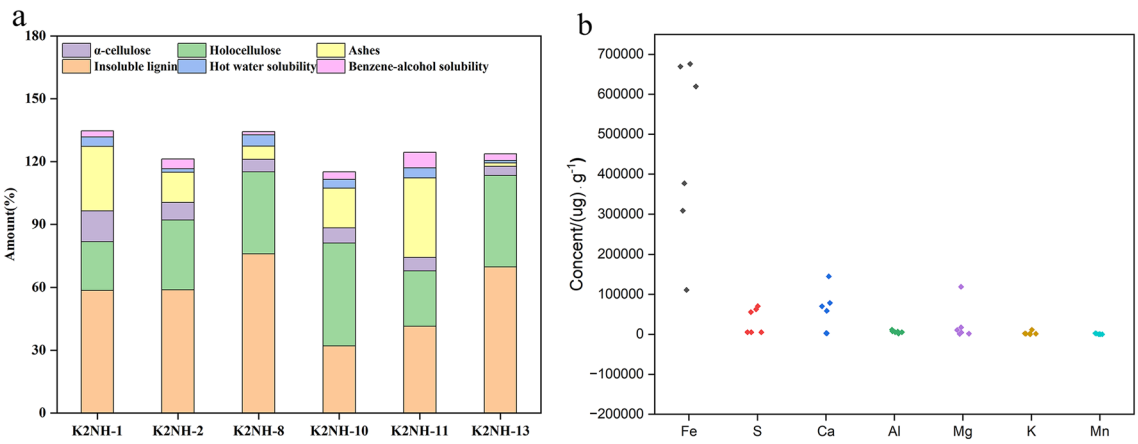

Fig. 4 Chemical composition (**a**) and element in ash (**b**) of Nanhai I samples

Table 3 Element in ash of Nanhai I samples by ICP-MS(μg/g)

Sample	Fe	S	Ca	Al	Mg	K	Mn	Mo
K2NH-1	30,878	62,768	145,000	6600	4880	1640	2120	4
K2NH-2	11,110	55,806	78,600	11,500	10,800	11,500	915	37
K2NH-8	377,005	70,529	70,300	7830	17,400	1480	2730	22
K2NH-10	619,440	5145	2970	5380	1230	1550	126	13
K2NH-11	669,512	5323	2610	2140	1690	123	155	4
K2NH-13	675,869	5413	58,800	5560	119,000	2240	125	54

Table 4 Elemental composition of wood samples (Weight/%)

Sample	C	H	O	N	S	O/C
K2NH-1	49.5	5.0	38.3	0.5	6.7	0.774
K2NH-2	52.5	5.6	37.6	0.4	3.9	0.716
K2NH-8	45.8	5.1	40.7	0.7	7.7	0.889
K2NH-10	43.6	5.4	47.5	0.4	3.1	1.089
K2NH-11	42.9	4.5	44.1	0.4	7.9	1.028
K2NH-13	55.8	4.7	34.5	0.5	4.6	0.618
Sound pine wood	49.9	6.3	42.9	1.0	0.2	0.860

samples are higher than sound pine wood (pH 4.3). Samples K2NH-1 and K2NH-2 were recently excavated from the sea mud and exposed to oxygen for the shortest time compared to other samples. Their pH values are 7.2 and 7.4 respectively, higher than other samples of a long time soaking in deionized water or EDTA-2Na solution. Compared with other samples, the ratios of O/C of samples K2NH-1 and K2NH-2 are relatively lower. The pH value may be related to the oxidation degree of the iron compounds in wood. Samples K2NH-1 and K2NH-2 were exposed to oxygen for the shortest time. It is speculated that iron deposits in the wood structure of samples K2NH-1 and K2NH-2 may be oxidized to the lowest degree, resulting in the pH of wood being closer to neutral pH.

Wood is mainly composed of three natural organic polymer substances: cellulose, hemicellulose, and lignin. Cellulose, hemicellulose, and lignin show characteristic infrared absorption bands in the "fingerprint" wavenumber region of 1800–800 cm^{-1} [31, 32]. Therefore, the degree of degradation of wood could be evaluated according to the fingerprint data (Fig. 5).

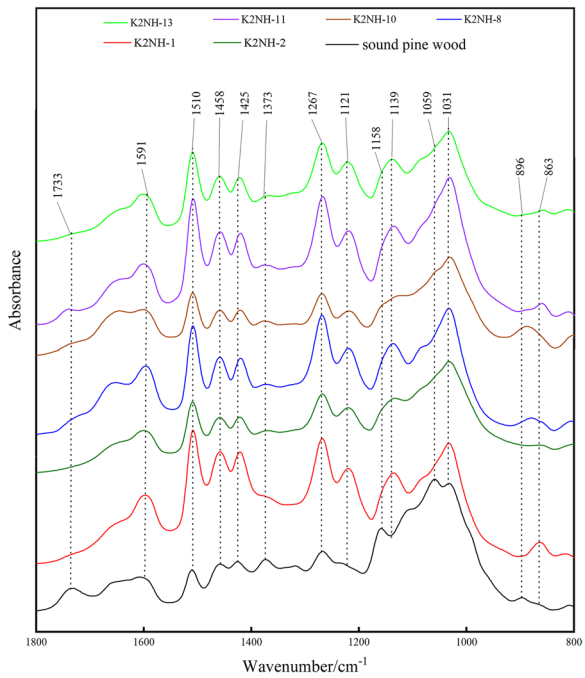

Fig. 5 Comparison of FTIR spectra of sound pine wood and degraded wood sample

Compared with sound pine wood, the C–H absorption band in cellulose at 896 cm^{-1} did not appear. Bands at 1373 cm^{-1}, of imputable C–H deformation in cellulose, the C–O–C, and C=O stretch at 1158 $cm^{-1}$and 1059 cm^{-1} did not appear, indicating that the cellulose and hemicellulose in the wood had been degraded [33, 34]. Aromatic skeletal vibrations at 1591 cm^{-1},1510 cm^{-1} and 1425 cm^{-1}, C–O–C vibrations in guaiacyl units at 1267 cm^{-1}, and C-H deformation at 1458 cm^{-1} signaled that those samples enriched with lignin in a relative sense [35]. It implies that the hemicellulose in Nanhai I waterlogged wood has been degraded, and the cellulose has been partially degraded [36, 37].

Deposits in wood microstructure

When the wood slices were observed under microscope, it could be seen a large amount of deposits in ray tracheids and axial tracheids. For example, in the cross-section and tangential sections of samples K2NH-10 (Fig. 6), red and black deposits are unevenly deposited in the wood cell lumen, middle lamella, and rays are full of a large amount of deposits. Fungal hyphae could be visible in tracheids (Fig. 6c).

The abundance and biodiversity of aerobic and anaerobic microorganisms were detected in the wood samples [38, 39] and desalination buffer [40] (deionized water with 10 mmol/L EDTA-2Na solution and 0.5% isothiazolinone K100) of Nanhai I shipwreck, among which advantage bacterium are *Hydrogenophaga*, *Lacibacter cauensis*, *Acidovorax delafieldii*, *Devosia*, *Sediminibacterium*, *Brevundimonas diminuta*, *Pseudomonas*, *Thiobacillus*, and *Flavobacterium,* etc. Among these bacteria, there are two types of marine bacteria in the wood associated with iron deposits formation in anaerobic condition: *Cytophagaceae* of erosion bacteria which participate in the degradation of wood [41], *Pseudomonas* of sulfate-reducing bacteria (SRB) which implicate in iron metabolism and enrichment of deposits [42, 43]. The enrichment of deposits in wood structures is related to the action of microorganisms [42, 44]. In anoxic and sulfate-rich environments, the microbial corrosion mechanism of iron (from iron artifacts) is mainly that SRB attacks iron via the withdrawal of electrons. Corrosion of iron by SRB is typically associated with the formation of iron sulfides (FeS). The stability of FeS is extremely poor, and under different oxygen and relative humidity conditions. It is converted into different iron compounds enrichment in wood structures.

Powder of wood samples was analyzed through XRD. According to the XRD results, there are deposits containing iron in wood samples of Nanhai I, such as pyrite (FeS_2), siderite ($FeCO_3$), goethite (FeOOH), and magnetite (Fe_3O_4). A typical XRD spectrum of sample K2NH-11 is shown in Fig. 7, and the specific analysis results are shown in Table 5 and Additional file 1.

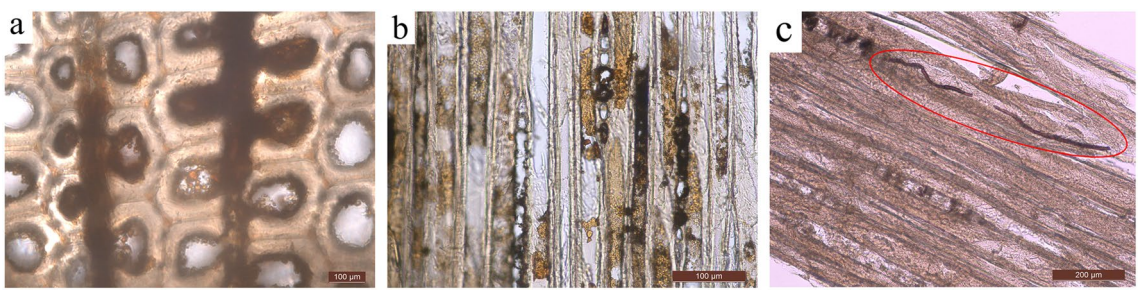

Fig. 6 Microscopic observation of sample K2NH-10 **a** cross-section, ×500; **b** tangential section, ×200; **c** tangential section, ×100

Iron artifacts were corroded mainly by SRB during the burial of Nanhai I shipwreck. The special product of SRB corrosion iron is mackinawite FeS, which is poor stability and can induce its transformation into greigite (Fe_3S_4) under exposure to sulfides. Fe_3S_4 can be converted to pyrite FeS_2. With the increase of exposure time of Nanhai I shipwreck in the oxygen, FeS_2 was oxidized to different iron compounds. FeS_2 can be transformed to $FeSO_4$, $Fe_2(SO_4)_3$, and FeOOH under aerobic and humid conditions. $FeCO_3$ is produced under anoxic environment [42, 44, 45]. The reduced iron sulfides are prone to oxidation in the presence of water, and sulfuric acids are generated. Sulfuric acid promotes further degradation of wood [17, 46]. Changes in temperature and humidity in the preservation environment make different iron compounds crystallize in wood structures [14]. This process can cause wood expansion and mechanical damage, and even block the microstructure of wood, seriously affect the penetration of protective materials [47].

Iron deposits in wood structures were also observed through SEM. From the images of SEM, different shapes of particles could be seen and enriched in the tangential section of the sample K2NH-10 (Figs. 8a, 9b) and cross-section of the sample of K2NH-11 (Fig. 8b, c). The results of EDS analysis are shown in Table 6. The results of the particles composition analysis of iron deposits in Figs. 8a, b and 9a show that Fe and S are the main elemental composition of iron deposit particles. The content of Fe is much higher than that of S of iron deposit particles. The EDS results showed that the molar ratio of Fe to S is between 2.9:1 to 19:1. The high iron content of deposits is supposed to be compounds of iron oxides (Figs. 8a, b, 9b, Table 6). In Fig. 8c, the molar ratio of Fe to S in particles is more than 2:1. Framboidal pyrite (FeS_2) was observed in wood samples collected of the Nanhai I shipwreck in 2011 and 2014. Elemental analysis showed that the ratio of Fe to S in pyrite particles was about 1:2 in 2011. Elemental analysis showed that the ratio of Fe to S in pyrite particles was about 2:1, or more than 2:1 and the oxygen content increased in 2014 [10]. With the extension of exposure time of Nanhai I shipwreck in the existence of oxygen,

Table 5 The result of iron deposits in wood samples

Sample	Types of iron deposits
K2NH-1	goethite, siderite, pyrite, quartz
K2NH-2	quartz
K2NH-8	pyrite, goethite
K2NH-10	magnetite, goethite
K2NH-11	pyrite, goethite, siderite, $Fe_2(SO_4)_3$
K2NH-13	–

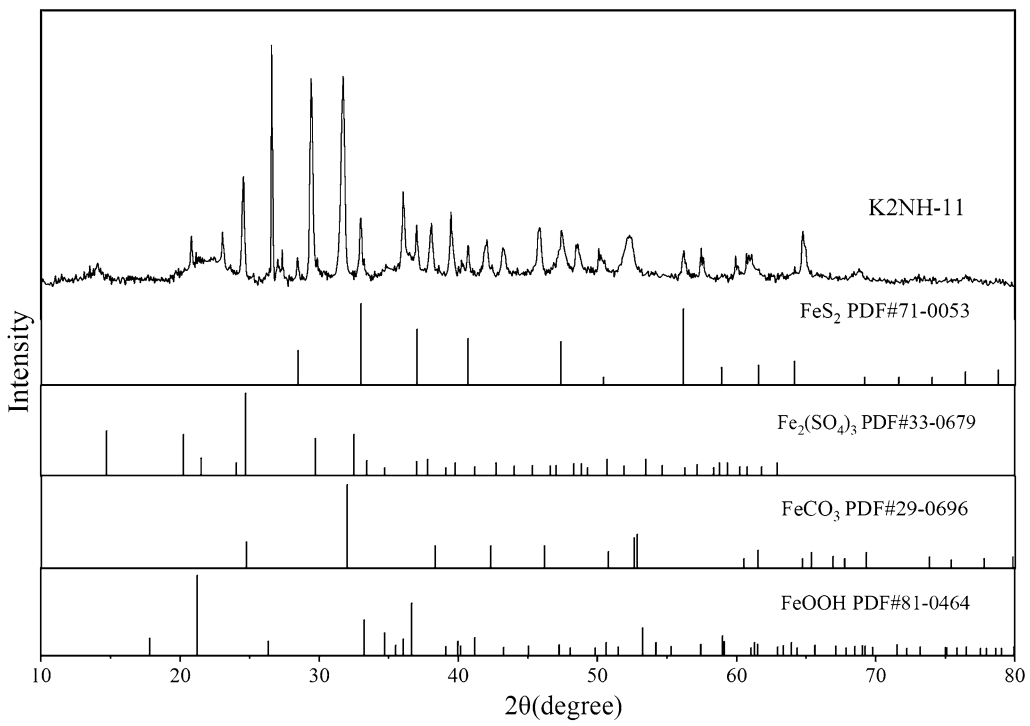

Fig. 7 XRD spectra of sample K2NH-11

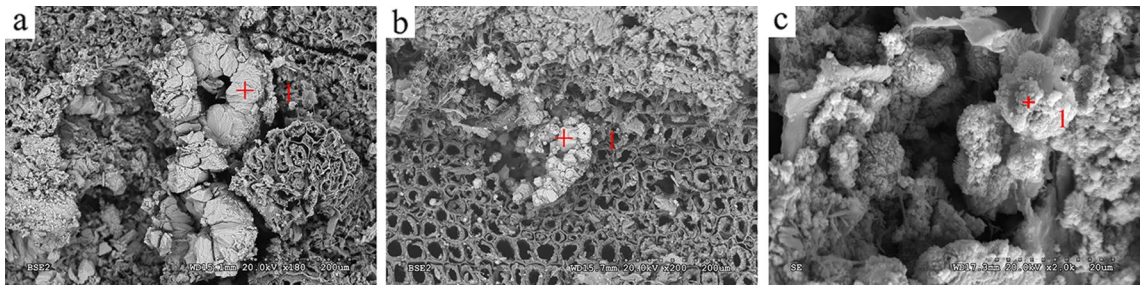

Fig. 8 SEM images of iron deposit in wood structure of Nanhai I shipwreck **a** SEM image of K2NH-10 sample; **b** SEM image of K2NH-11 sample; **c** SEM image of K2NH-11sample

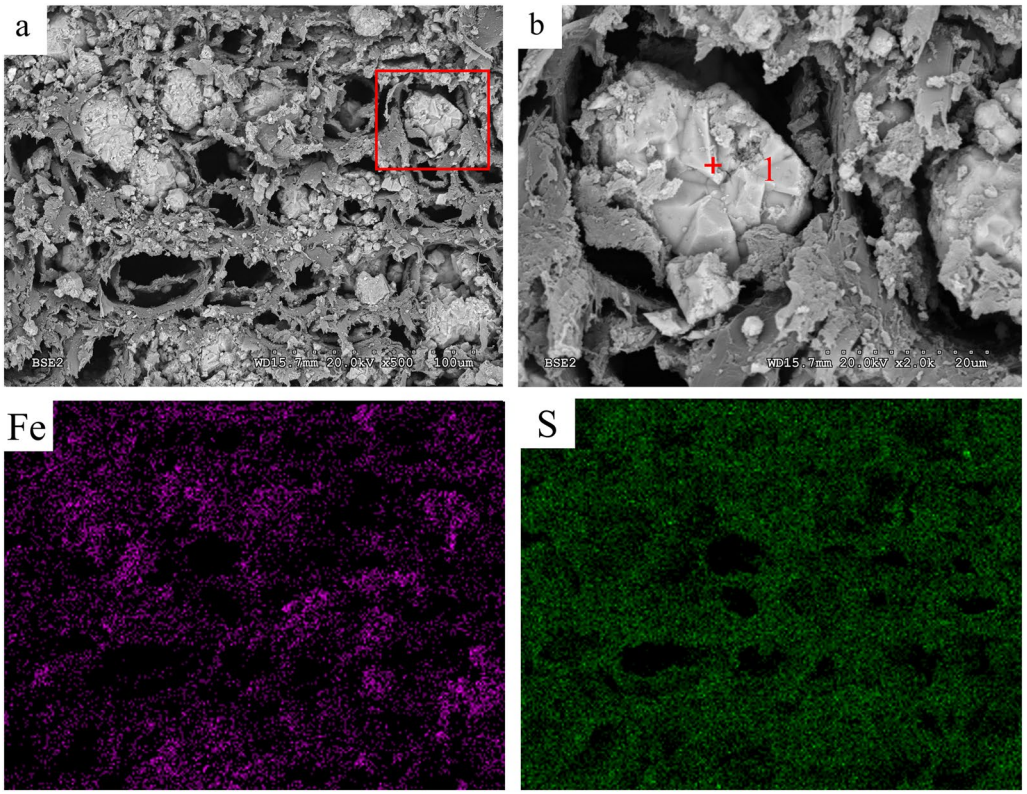

Fig. 9 K2NH-10 cross profile element mapping

Table 6 SEM–EDS results of iron deposit (at.%) in Figs. 8 and 9

Sample	Analyzed point	C	O	Fe	Na	Mg	Al	Si	S	K	Ca
K2NH-10	Figure 8a-1	36.71	20.67	20.67	1.38	0.90	0.60	0.77	2.10	0.00	0.39
K2NH-11	Figure 8b-1	73.90	6.76	14.48	0.19	0.38	0.22	0.49	3.44	0.03	0.11
K2NH-11	Figure 8c-1	54.08	6.19	28.42	0.00	0.23	0.16	0.71	9.96	0.00	0.25
K2NH-10	Figure 9b-1	30.83	10.72	49.19	1.67	1.40	1.02	2.25	2.59	0.14	0.19

although pyrite was maintained as microscopic spheroidal, the surface of particles had been oxidized.

There were differences in morphology of deposits of iron compounds in wood structure. Microcrystal geometries of framboidal pyrite is closely related to the S/Fe ratio in sedimentary environment. Microcrystal geometries of framboidal pyrite usually have cube, octahedron, and spherulite [48, 49]. The oxidation products of pyrite are usually ferric oxyhydroxides and iron-sulphate containing compounds. The oxidation products of pyrite are similar to pyrite in microcrystal geometries and particle size distribution [50]. Iron oxides and oxyhydroxides are also important iron-bearing minerals in marine deposits and conclude goethite, hematite, and magnetite. Microcrystal geometries of goethite are needle-shaped, cube, hexagonal flake-like, etc. Microcrystal geometries of hematite are hexagonal flake-like, rhombohedron, and spherical [51].

Elemental mapping of sample K2NH-10 reveals the coexistence of S and Fe in deposit particles (Fig. 9), and the iron content of deposit particles in the wood structure is higher than S (Fig. 9b).

According to the analysis results of XRD and SEM–EDS of sample K2NH-11, iron compounds still exist in wood structure after 20 months of iron deposits removal. Compared with sample K2NH-10, the content of O in iron deposit particles of sample K2NH-11 was relatively lower, and the content of S was relatively higher. It was speculated that after soaking in EDTA-2Na solution, some oxidized iron compounds on the particle surface in wood structure of sample K2NH-11 were partially dissolved.

Micro-XRF mapping exhibited meaningful enrichment assessment of the distribution and relative content of iron and sulfur of the exterior and interior of sample K2NH-10. The sample block was cut from sample K2NH-10, 2 cm from the transverse surface, and vacuum freeze-dried. After drying, the color of sample exterior is unevenly red (Fig. 10a). Iron deposits had diffused and deposited into the wood structure, resulting in brownish-black color of interior of wood (Fig. 10b). The ordinate of micro-XRF mapping represented respectively the relative signal intensity of Fe and S on the exterior and interior of sample K2NH-10. The more red color in the mapping

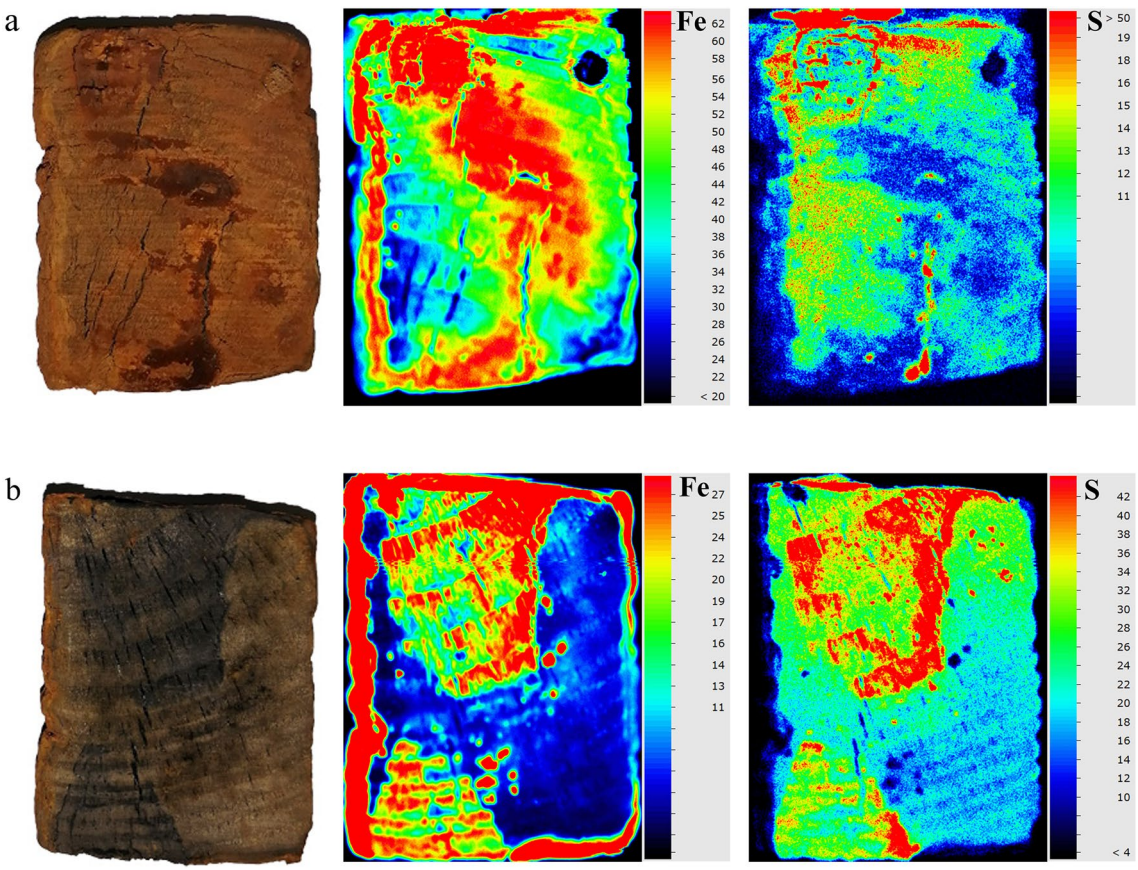

Fig. 10 The distribution and relative content of iron and sulfur **a** exterior of sample; **b** interior of sample

was shown the stronger the signal of Fe or S at this position in the wood structure. That means the higher relative content of Fe or S at this position in the wood structure. The sample exterior and interior contain a large number of unevenly and inconsistent distributed Fe and S. There was an obvious difference in content between Fe and S on the sample exterior and interior. Compared to the interior of sample, the iron content is higher and the sulfur content is relatively low of exterior of the sample. No matter exterior and interior of wood sample, Fe was inclined to be enriched on the edge of wood, while S was inclined to be enriched inside of wood. In the marine burial environment, the corrosion products of iron artifacts had penetrated from the exterior to the interior of wood structure. The distribution characteristics of iron content in wood are relatively higher in the exterior and relatively lower in the interior. After the wood enriched with iron deposits was salvaged and exposed to oxygen, the Fe(II) sulfides near the exterior in the wood structure were oxidized to FeOOH, $Fe_2(SO_4)_3$, and sulfuric acid. During the immersion in deionized water, the soluble SO_4^{2-} in the exterior of wood structure was removed, so that the sulfur content of sample exterior was relatively lower.

Conclusions

Nanhai I shipwreck was originally loaded with a large number of iron artifacts, which had almost occurred corrosion while underwater, and their corrosion products had diffused into the wood structure. The presence of iron compounds can accelerate degradation and increase safety hazards of shipwreck and waterlogged wood in the preservation process.

Samples of loose wood from Nanhai I shipwreck are used to evaluate the degradation state to select the appropriate protection method. Through chemical components, element analysis, and FTIR spectroscopy, the cellulose has also undergone partial degradation. These results indicate a high degree of wood degradation of the Nanhai I shipwreck. The ash content of Nanhai I shipwreck is relatively higher than sound wood due to the enrichment of deposits in the wood structure. The main inorganic metallic element of ash is Fe.

The waterlogged wood from Nanhai I shipwreck was enriched with iron deposits to varying degrees. Analysis of iron deposit particles in the wood structure and relatively content of exterior and interior of wood suggests that iron deposits content of Fe is higher than S. Large amounts of iron deposits are present in the wood of Nanhai I shipwreck in the form of mainly iron oxides and hydroxides. The degree of enrichment of iron deposits varies between samples and is related to the degree of contamination of iron artifacts rustiness during the burial of Nanhai I shipwreck. The distribution of iron deposits in wood structures is unevenly deposited in the wood cell lumen, middle lamella, and rays. The iron content is higher and the sulfur content is relatively low on exterior of the sample.

Considering the characteristic of iron deposits, the presence of iron deposits in wood has seriously led to acidification, degradation, and mechanical damage of marine archaeological wood. The analysis characterization of degradation and iron deposits of the wood of Nanhai I shipwreck provides a foundation for the selection of materials for removing iron deposits in the conservation process of Nanhai I shipwreck, which is also the first stage of work of our team. Our research idea is to use complexing agents, oxidizing and reducing agents, and combinations of these chemicals to remove iron deposits from the wood of Nanhai I shipwreck. The efficiency of removing Fe element from wood is currently being systematically evaluated. The study report on the removal of iron deposits from wood of Nanhai I shipwreck will be published in succession.

Abbreviations

MWC: Maximum water content; BD: Basic density; RBD: Residual basic density; H/L: The ratios of holocellulose and lignin; O/C: The ratio of oxygen to carbon; ICP-MS: Inductively coupled plasma mass spectrometry; SEM–EDS: Scanning electron microscope–X-ray energy dispersive spectroscopy; FTIR: Fourier transforms infrared spectroscopy; XRD: X-ray diffraction; micro-XRF: Micro-X-ray fluorescence.

Supplementary Information

The online version contains supplementary material available at https://doi.org/10.1186/s40494-022-00845-9.

Additional file 1: Figure S1. XRD spectra of sample K2NH-1. **Figure S2.** XRD spectra of sample K2NH-2. **Figure S3.** XRD spectra of sample K2NH-8. **Figure S4.** XRD spectra of sample K2NH-10.

Acknowledgements

The authors express their gratitude to Miss Fengdan Hu at the China Academy of Cultural Heritage, Professor Yanxiang Li, Professor Kunlun Chen, and associate Professor Xiangna Han, etc., at the University of Science and Technology Beijing for their kind support and assistance with this research. Wood samples were supplied by the Maritime Silk Road Museum of Guandong.

Author contributions

QM provided support and guidance for this study. HZ and DS performed experiment analysis and drafted the manuscript. ZZ provided assistance in the study. All authors read and approved the final manuscript.

Funding

This research is funded by China's National Key R&D Program (2020YFC1521802).

Availability of data and materials

All data analyzed during this study are available from the corresponding author on request.

Declarations

Competing interests

The authors declare that they have no competing interests.

Author details

[1]Institute of Cultural Heritage and History of Science & Technology, University of Science and Technology Beijing, Beijing 100083, China. [2]China Academy of Cultural Heritage, Beijing 100029, China. [3]National Centre for Archaeology, Beijing 100013, China. [4]International Joint Research Laboratory of Environmental and Social Archaeology, Shandong University, Qingdao 266237, Shandong Province, China.

Received: 1 June 2022 Accepted: 12 December 2022
Published online: 20 December 2022

References

1. Sun J. Archaeological summary of the Song Dynasty shipwreck Nanhai I in China. Natl Mar Res. 2020;1:55–76 (**in Chinese**).
2. North NA, MacLeod ID. Corrosion of metals. In: Pearson C, editor. Conservation of marine archaeological objects. Amsterdam: Butterworth-Heinemann; 1987. p. 77.
3. Almkvist G, Persson I. Distribution of iron and sulfur and their speciation in relation to degradation processes in wood from the Swedish warship Vasa. New J Chem. 2011;35:1491–502. https://doi.org/10.1039/C1NJ20056A.
4. Smith AD, Jones M, Berko A, Chadwick AV, Newport RJ, et al. An investigation of the Sulfur–Iron chemistry in timbers of the sixteenth century warship, the Mary Rose, by Synchrotron micro-X-ray spectroscopy. In: Turbanti-Memmi I, editor. Proceedings of the 37th international symposium on archaeometry, 13th–16th May 2008, Siena, Italy. 2011. p. 389–394. https://doi.org/10.1007/978-3-642-14678-7_56.
5. Sandström M, Jalilehvand F, Damian E, Fors Y, Gelius U, Jones M, Murielle S. Sulfur accumulation in the timbers of King Henry VIII's warship Mary Rose: a pathway in the sulfur cycle of conservation concern. In: Proceedings of the National Academy of Sciences, USA. 2005. p. 14165–14170. https://doi.org/10.1073/pnas.0504490102.
6. Bettazzi F, Giachi G, Staccioli G, Chimichi S. Chemical characterisation of wood of Roman Ships brought to light in the recently discovered ancient Harbour of Pisa (Tuscany, Italy). Holzforschung. 2003;57:373–6. https://doi.org/10.1515/HF.2003.055.
7. Remazeilles C, Tran K, Guilminot E, Conforto E, Refait P. Study of iron (II) sulphides by environmental scanning electron microscopy (ESEM) and micro-Raman spectroscopy in waterlogged archaeological woods. In: International conference on non-destructive investigations & microanalysis for the diagnostics & conservation of cultural & environmental heritage. 2011. p. 297–307. https://doi.org/10.13140/2.1.3740.1282.
8. Macleod ID. Conservation of waterlogged timbers from the Batavia 1629. Bull Aust Inst Marit Archaeol. 1990;14:1–8.
9. Rémazeilles C, Meunier L, Lévêque F, Plasson N, Conforto E, et al. Post-treatment study of Iron/Sulfur-containing compounds in the wreck of Lyon Saint-Georges 4 (Second Century ACE). Stud Conserv. 2019;65:28–36. https://doi.org/10.1080/00393630.2019.1610608.
10. Shen DW. Iron sulfide of marine archaeological wood. Beijing: China Science Publishing; 2020. p. 49–55 (**in Chinese**).
11. Shen DW, Li NS, Fu Y, Macchioni N, Sozzi L, et al. Study on wood preservation state of Chinese ancient shipwreck Huaguangjiao I. J Cult Herit. 2018;32:53–9. https://doi.org/10.1016/j.culher.2018.01.009.
12. Tian XL, Li NS, Zhang ZG, Shen DW, Liu J. Analysis and research on the wood from the Ming Dynasty shipwreck, Nan'ao No.1, in Shantou city, Guangdong. Sci Conserv Archaeol. 2014. https://doi.org/10.16334/j.cnki.cn31-1652/k.2014.04.018. (**in Chinese**).
13. Zhang ZG, Li NS, Tian XL, Liu J, Shen DW. Research on the removal of the iron sulfides in the Qing Dynasty marine shipwreck, Ningbo Xiaobaijiao No. 1. Sci Conserv Archaeol. 2014;26:30–8. https://doi.org/10.16334/j.cnki.cn31-1652/k.2014.04.006.
14. Lindfors EL, Lindström M, Iversen T. Polysaccharide degradation in waterlogged oak wood from the ancient warship Vasa. Holzforschung. 2008;62:57–63. https://doi.org/10.1515/HF.2008.008.
15. Bjurhager I, Halonen H, Lindfors EL, Iversen T, Almkvist G, et al. State of degradation in archeological oak from the 17th century Vasa ship: substantial strength loss correlates with reduction in (holo)cellulose molecular weight. Biomacromol. 2012;13:2521–7. https://doi.org/10.1021/bm3007456.
16. Rémazeilles C, Tran K, Guilminot E, Conforto E, Refait P. Study of Fe (II) sulphides in waterlogged archaeological wood. Stud Conserv. 2013;58:297–307. https://doi.org/10.1179/2047058412Y.0000000071.
17. Almkvist G, Persson I. Fenton-induced degradation of polyethylene glycol and oak holocellulose. A model experiment in comparison to changes observed in conserved waterlogged wood. Holzforschung. 2008;62(6):704–8. https://doi.org/10.1515/HF.2008.129.
18. Shi SL, He FW. Analysis and inspection of pulp and paper. Beijing: China Light Industry Press; 2010. p. 109–15 (**in Chinese**).
19. Macchioni N. Physical characteristics of the wood from the excavations of the ancient port of Pisa. J Cult Herit. 2003;4:85–9. https://doi.org/10.1016/S1296-2074(03)00019-0.
20. National Technical Committee 141 on Paper Industry of Standardization Administration of China. Fibrous raw material—Determination of ash, in: Paper industry test method standard manual, Beijing, National Paper Standardization Center (**in Chinese**)
21. Macchioni N, Pizzo B, Capretti C, Giachi G. How an integrated diagnostic approach can help in a correct evaluation of the state of preservation of waterlogged archaeological wooden artefacts. J Archaeol Sci. 2012;39:3255–63. https://doi.org/10.1016/j.jas.2012.05.008.
22. Jensen P, Gregory DJ. Selected physical parameters to characterize the state of preservation of waterlogged archaeological wood: a practical guide for their determination. J Archaeol Sci. 2006;33:551–9. https://doi.org/10.1016/j.jas.2005.09.007.
23. McConnachie G, Eaton R, Jones M. A re-evaluation of the use of maximum moisture content data for assessing the condition of waterlogged archaeological wood. Environ Sci. 2008;5:29–35.
24. Babiński L, Izdebska-Mucha D, Waliszewska B. Evaluation of the state of preservation of waterlogged archaeological wood based on its physical properties: basic density vs. wood substance density. J Archaeol Sci. 2014;46:372–83. https://doi.org/10.1016/j.jas.2014.03.038.
25. Kiliç AG, Kiliç N. Application of FTIR spectroscopy to the characterization of waterlogged archaeological woods of three galleys from YENİKAPI, İSTANBUL: contribution to conservation. Mediterr Archaeol Archaeom. 2021;21:93–105. https://doi.org/10.5281/zenodo.4681734.
26. High KE, Penkman KEH. A review of analytical methods for assessing preservation in waterlogged archaeological wood and their application in practice. Herit Sci. 2020;8:83. https://doi.org/10.1186/s40494-020-00422-y.
27. Editing G. The study of wood science. Beijing: China Forestry Publishing House; 1997. p. 31 (**in Chinese**).
28. Xiaochen M. Damage analysis and study on micro deterioration and protection of material properties of Yingxian Wooden Pagoda. Taiyuan Univ Technol 2021;78–95 (**in Chinese**)
29. Pinder AP, Panter I, Abbott GD, Keely BJ. Deterioration of the Hanson Logboat: chemical and imaging assessment with removal of polyethylene glycol conserving agent. Sci Rep. 2017;7:13697. https://doi.org/10.1038/s41598-017-14057-w.
30. Spiker EC, Hatcher PG. The effects of early diagenesis on the chemical and stable carbon isotopic composition of wood. Geochim Cosmochim Acta. 1987;51:1385–91. https://doi.org/10.1016/0016-7037(87)90323-1.
31. Yvonne F, Farideh J, Magnus S. Analytical aspects of waterlogged wood in historical shipwrecks. Anal Sci. 2011;27:785–92. https://doi.org/10.2116/analsci.27.785.
32. Almkvist G, et al. Prediction of tensile strength in iron-contaminated archaeological wood by FT-IR spectroscopy—a study of degradation in recent oak and Vasa oak. Holzforschung. 2016;70(9):855–65. https://doi.org/10.1515/hf-2015-0223.
33. Herrera R, Erdocia X, Llano-Ponte R, Labidi J. Characterization of hydrothermally treated wood in relation to changes on its chemical composition and physical properties. J Anal Appl Pyrol. 2014;107:256–66. https://doi.org/10.1016/j.jaap.2014.03.010.
34. Pizzo B, Pecoraro E, Macchioni N. A new method to quantitatively evaluate the chemical composition of waterlogged wood by means of

attenuated total reflectance Fourier transform infrared (ATR FT-IR) measurements carried out on wet material. Appl Spectrosc. 2013;67:553–62. https://doi.org/10.1366/12-06819.
35. Kubovský I, Kačíková D, Kačík F. Structural changes of oak wood main components caused by thermal modification. Polymers (Basel). 2020;12(2):485. https://doi.org/10.3390/polym12020485.
36. Popescu CM, Popescu MC, Singurel G, Vasile C, Argyropoulos DS, et al. Spectral characterization of eucalyptus wood. Appl Spectrosc. 2007;61(11):1168–77. https://doi.org/10.1366/000370207782597076.
37. Traore M, Kaal J, Cortizas MA. Application of FTIR spectroscopy to the characterization of archeological wood. Spectrochim Acta A Mol Biomol Spectrosc. 2016;153:63–70. https://doi.org/10.1016/j.saa.2015.07.108.
38. Liu ZJ, Fu TT, Hu CT, Shen DW, Macchioni N, et al. Microbial community analysis and biodeterioration of waterlogged archaeological wood from the Nanhai No. 1 shipwreck during storage. Sci Rep. 2018;8:1–11. https://doi.org/10.1038/s41598-018-25484-8.
39. Li QX, Cao LX, Tan HM, Sun J, Cui Y, et al. Bacterial communities in the waterlogged wooden cultural relics from the "Nanhai No1" shipwreck. Acta Microbiol Sin. 2018;58:1439–52. https://doi.org/10.13343/j.cnki.wsxb.20170488. (**in Chinese**).
40. Han YQ, Du J, Huang XD, Ma KX, Wang Y, et al. Chemical properties and microbial analysis of waterlogged archaeological wood from the Nanhai No. 1 Shipwreck. Forests. 2021. https://doi.org/10.3390/f12050587.
41. Bjordal CG, Nilsson T, Daniel G. Microbial decay of waterlogged archaeological wood found in Sweden applicable to archaeology and conservation. Int Biodeterior Biodegradation. 1999;43:63–73. https://doi.org/10.1016/S0964-8305(98)00070-5.
42. Enning D, Garrelfs J. Corrosion of iron by sulfate-reducing bacteria: new views of an old problem. Appl Environ Microbiol. 2014;80:1226–36. https://doi.org/10.1128/AEM.02848-13.
43. Landy ET, Mitchell JI, Hotchkiss S, Eaton RA. Bacterial diversity associated with archaeological waterlogged wood: Ribosomal RNA clone libraries and denaturing gradient gel electrophoresis (DGGE). Int Biodeterior Biodegradation. 2008;61:106–16. https://doi.org/10.1016/j.ibiod.2007.07.007.
44. Rémazeilles C, Lévêque F, Conforto E, Refait P. Long-term alteration processes of iron fasteners extracted from archaeological shipwrecks aged in biologically active waterlogged media. Corros Sci. 2021;181:1–12. https://doi.org/10.1016/j.corsci.2020.109231.
45. Yang XY, Gong YM. Pyrite framboid: indicator of environments and life. Earth Sci J China Univ Geosci. 2011;36:644–58 (**in Chinese**).
46. Fors Y, Sandström M. Sulfur and iron in shipwrecks cause conservation concerns. Chem Soc Rev. 2006;35(5):399–415. https://doi.org/10.1039/b507010b.
47. MacLeod ID, Kenna C. Degradation of archaeological timbers by pyrite: oxidation of iron and sulphur species. In: Proceedings of the 4th ICOM group on wet organic archaeological materials conference. 1990. p. 133–143.
48. Li HX, Lu XC, Bian LZ, Xu WW, Juan L. Formation of pyrite framboids in the chamber of foraminiferas and its geological significance: a case study of the foraminiferas fossils in the qixia formation in the yanmenkou area Hubei Province. Geol J China Univ. 2009;15:470–6. https://doi.org/10.1016/S1874-8651(10)60080-4. (**in Chinese**).
49. Wang QW, Morse JW. Pyrite formation under conditions approximating those in anoxic sediments I. Pathway and morphology. Mar Chem. 1996;52:99–121. https://doi.org/10.1016/0304-4203(95)00082-8.
50. Chang XL, Huang YG, Chen ZQ, Hou MC. The microscopic analysis of pyrite framboids and application in paleo-oceanography. Acta Sedimentol Sin. 2020;38:150–65. https://doi.org/10.14027/j.issn.1000-0550.2019.099. (**in Chinese**).
51. Cornell RM. The iron oxides: structure, properties, reactions, occurrences and uses. Weinheim: Wiley-VCH; 2003. p. 9–38.

Publisher's Note